Inclusion of the physical wind tunnel in vehicle CFD simulations for improved prediction quality

Inclusion of the physical wind tunnel in vehicle CFD simulations for improved prediction quality

Emil Ljungskog
Department of Mechanics and Maritime Science
Chalmers University of Technology
Gothenburg, Sweden
emil.ljungskog@chalmers.se

Simone Sebben
Department of Mechanics and Maritime Science
Chalmers University of Technology
Gothenburg, Sweden
simone.sebben@chalmers.se

Alexander Broniewicz
Aerodynamics
Volvo Cars
Gothenburg, Sweden
alexander.broniewicz@volvocars.com

Abstract

When performing numerical simulations of the aerodynamic properties of vehicles, the simulation domain used is often a large box with a very low blockage ratio and a fully moving ground plane, replicating open road conditions. However, the physical measurements to which the simulation results are usually compared are typically performed in wind tunnels, with deficiencies concerning blockage, ground modeling, and other boundary interference effects. Some of these effects can be corrected for, but such corrections are usually performed on a global level and thus fail to correct for local effects that might influence different configurations of the vehicle in different ways. In this work, the typical open road numerical setup is compared to simulations where the computational domain is a virtual model of the complete slotted wall wind tunnel test section geometry. A vehicle of sedan type is simulated in different configurations, and the simulation results are compared to forces and pressure measurements from physical tests. The results show that the absolute drag coefficient can be predicted with very good accuracy by simulating the car inside the wind tunnel if compared to uncorrected measurement data. However, despite the good agreement for drag, the prediction of lift is not as satisfactory.

***K*eywords** Wind Tunnel, Wind Tunnel Simulation, Vehicle Aerodynamics, CFD

1 Introduction

Numerical simulations of the aerodynamical performance of vehicles are frequently used in the industry today to evaluate and optimize the vehicle design. In order to fully trust the results of such Computational Fluid Dynamics (CFD) simulations, they have to be validated by comparison to test data, usually obtained from a wind tunnel. When differences occur between test and simulation, they can typically be attributed to at least one of three broad categories:

1. Shortcomings of the numerical modeling
2. Uncertain geometrical representation of the test object
3. Different test domains and boundary conditions

Significant advances have been made regarding item 1, with scale-resolving methods being developed and becoming feasible with increasing computational power. Furthermore, the rise of 3D-scanners has improved the possibility of ensuring that the CAD data used as input to the simulations are representative of the physical test object, thus alleviating some of the uncertainties regarding item 2.

Regarding item 3, the common way of running vehicle aerodynamic CFD simulations is using open road conditions, where the numerical test domain is a large rectangular cuboid with a uniform inlet flow, fully moving ground plane and negligible blockage ratio. This is not very similar to the test section of a wind tunnel, where the blockage ratio is typically on the order of 10 %, the flow is not fully uniform, and the movement of the ground relative to the car has to be simulated using different techniques usually covering only the area under and just in front of the vehicle. A common way of accounting for the difference caused by the wind tunnel interference is to adjust the physical measurements using correction methods often based on inviscid flow theory.

Instead of correcting the physical measurements to supposedly match open road conditions, it is possible to find the correlation between tests and simulations by including the wind tunnel geometry in the numerical simulations. This approach has previously been attempted, with some examples available in the literature. Fischer et al. [1–3] investigated the blockage correction for an open jet wind tunnel by simulating both simplified geometries [1] and detailed scale model vehicles [2, 3]. For most of the tested configurations, they did achieve improved force predictions when comparing uncorrected wind tunnel data to simulations of the vehicle in the test section, in contrast to comparing open road simulations to corrected wind tunnel data. They also noted that some parts of the correction method for the physical measurements were overpredicting the boundary interference. The same open jet tunnel was also studied by Cyr et al. [4], who compared drag values for a detailed scale model sedan in different underbody configurations. They found that including the wind tunnel geometry and the different ground simulation systems can result in very good agreement with physical measurements. In a study by Collin et al. [5], the DrivAer reference body was simulated in a simplified open jet tunnel in order to investigate blockage effects from varying nozzle sizes. The authors noted that the correlation between physical measurements and simulation was good for drag when the stings holding the model and wheels in the wind tunnel were included in the wind tunnel, but that lift was harder to predict.

For slotted wall test sections, investigations using steady-state Reynolds Averaged Navier-Stokes (RANS) methods have previously been published by Perzon [6], Olander [7] and Wall [8]. They all noted that the inclusion of the wind tunnel geometry in the simulations had a significant impact on the forces, but the agreement with measurements was not consistently improved compared to open road simulations. This can likely be attributed to shortcomings in the numerical method, as well as issues regarding the non-dimensionalization of the force coefficients.

The present work aims at improving the correlation between numerical simulations and physical measurements from a slotted wall wind tunnel, in terms of the prediction of the forces and surface pressures on a sedan type of vehicle. This is done by simulating the vehicle in several configurations, both in open road conditions as well as in a virtual model of the wind tunnel, using scale resolving simulation techniques. The results obtained are then compared to physical measurements of forces, and surface pressures on the vehicle centerline and its rear base.

Table 1: Force coefficient repeatability in the physical wind tunnel.

Force	Coefficient	Repeatability	
		Within test	Between tests
Drag	C_D	±0.001	±0.003
Front lift	C_{LF}	±0.001	±0.008
Rear lift	C_{LR}	±0.005	±0.008

2 Method

The methods used for both physical measurements and numerical simulations are described in this section, beginning with a description of the test facility, test object and performed measurements. This is followed by an introduction to the simulation method, with a particular focus on the simulations of the car inside the virtual model of the physical wind tunnel.

2.1 Physical measurements

The physical wind tunnel used for the measurements was the Volvo Cars Aerodynamic Wind Tunnel (PVT) in Gothenburg, Sweden. It is of Göttingen type with a slotted wall test section with a cross-sectional area of 27 m^2 and a slot open area ratio of 30 %. All tests were run at a wind speed of 140 km/h at zero yaw. Forces were measured using the underfloor balance, and the repeatability of the force coefficients are given in Table 1. The reason for the different behaviors of the front and rear lift coefficients is that the repeatability between tests is mostly determined by the installation of the vehicle, which might differ slightly between tests. On the other hand, the repeatability within a test is mostly determined by unsteady flow behavior over the car and thus the averaging time. The front of the car is subjected to a very steady oncoming flow, and hence the front lift is quite steady, whereas the rear lift is more affected by the unsteady flow under the car in in the base wake. It would thereby be possible to improve the within test repeatability for rear lift by averaging the forces over a longer time. The averaging time used in this work was 20 s, which is the averaging time used for regular vehicle development work, and was chosen as a reasonable trade-off between repeatability and productivity.

The tunnel is equipped with a ground effect simulation system consisting of scoop suction, distributed suction and tangential blowing for boundary layer control, as well as a five belt moving ground system providing wheel rotation and relative motion between the vehicle and the ground. An outline of the ground effect simulation system is shown in Figure 1, where it can be seen that the distributed suction, which prevents a boundary layer build-up by suction through more than 100 000 holes in the perforated floor, is split into two parts. The second part is mounted on the turntable together with the moving belts and tangential blowers, which acts to refill the momentum deficit by blowing air tangential to the floor at high speed through 0.6 mm to 1.0 mm tall slots. The wheel drive unit (WDU) belts and the corresponding blowers, as well as the rocker panel restraint posts holding the car in place during a test, can be moved both laterally and longitudinally in order to accommodate vehicles of different track width and wheelbase. More thorough descriptions of the tunnel and its moving ground system, including flow quality data from the wind tunnel commissioning, were given by Sternéus et al. [9] and Ljungskog [10].

While the centerbelt installation is not connected to the underfloor balance, the wheel drive units have to be in order to measure lift on the vehicle. Thus, a spurious lift force will be measured if a pressure difference is present between the upper side of the WDU, facing the test section, and the lower side located in the balance room under the test section floor. In the presence of a wheel on the WDU, the pressure field will be affected on the test section side, thus introducing such a pressure difference. For the corrected data from the physical wind tunnel, this effect is taken into account using a CFD based approach developed by Eng [11], which used a simplified tire geometry to compute the pressure field on the upper WDU surface.

2.1.1 Test object

The test object was a production Volvo S60 of model year 2010, which had been modified with a stiff suspension, removed drive shafts, closed cooling inlets, and taped split lines. This particular test object has been described in some detail by Hobeika [12] and Bonitz [13] in other related studies. Figure 2 shows the vehicle mounted in the test section of the physical wind tunnel. The wheels used had slick tires with cut rain grooves mounted on 17-inch production rims, as described by Hobeika and Sebben [14, 15]. They were

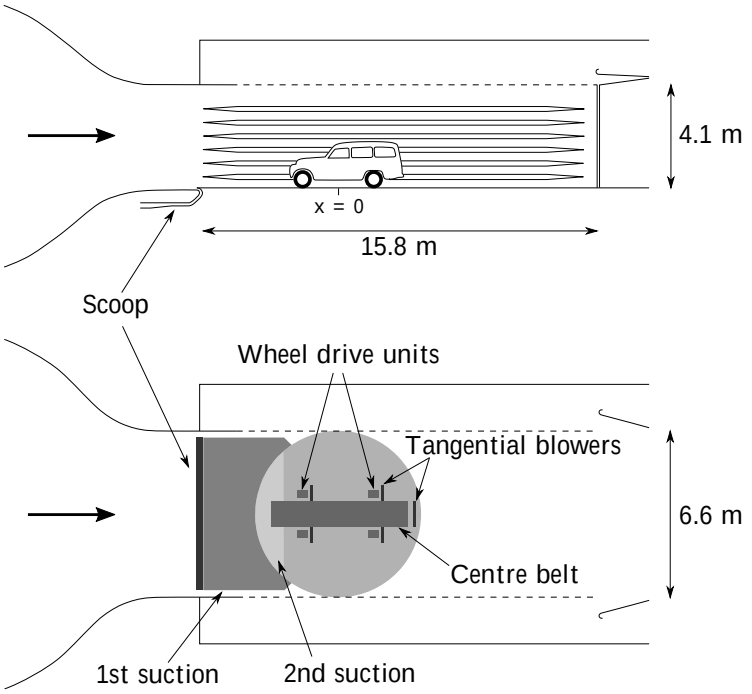

Figure 1: General layout of the ground effect simulation system in Volvo PVT.

used in order to simplify the modeling of the wheel rotation in the subsequent numerical simulations. Apart from this baseline configuration (Figure 2a), the vehicle was also tested with its front wheel deflectors (b) removed, with covered rims (c), and without rearview mirrors (d).

The vehicle was instrumented with pressure taps on the rear base and on the tophat centerline. A total of 122 drilled and sticker taps were used, of which 40 on the centerline and 82 on the base. All taps were connected to PSI ESP pressure scanners inside the car, and all data were averaged for 20 s.

2.2 Numerical method

For the numerical simulations, two different domains were used, as described in Section 2.2.1. All simulations were run in STAR-CCM+ using the SST k-ω Improved Delayed Detached Eddy Simulation (IDDES) turbulence model [16] with the so-called All y+ wall treatment. The flow was initialized with a steady-state solution, and allowed to develop for 2.6 s before averaging for 1.4 s. The time step was 2.5×10^{-4} s, which resulted in CFL numbers below unity in the majority of the domain, with only a small number of cells with CFL numbers above 50. This is expected to yield good accuracy as shown by Ekman et al. [17] for a similar method, and by Hobeika and Sebben [15] for the same test object. The modeling of the rotation of the rims was done using a sliding mesh approach, while the tire rotation was provided by a rotating wall condition. To account for the tire deformation at the contact patch, the tire geometry used in the simulations had been morphed to match the shape of a loaded physical tire, with different geometries for front and rear due to the different loads, camber, and toe on the axles. The morphed tire geometries were intersected with the ground to result in contact patch sizes matching those of the physical vehicle. These techniques have previously been shown to yield good predictions of the flow around the wheels [12, 14, 15].

2.2.1 Computational domains

The computational domain used for the open road simulations is shown in Figure 3a, and consisted of a rectangular box of dimensions 70 m × 40 m × 30 m, thus yielding a blockage ratio of less than 0.3 %. A uniform velocity profile was used as the inlet condition, while the outlet was set as a pressure outlet. Movement of the full ground plane was introduced using a moving wall boundary condition, while the sides and the top of the domain were set as symmetry planes. The inlet velocity of 140 km/h and the outlet gauge pressure of 0 Pa were used as reference values for the non-dimensionalized forces and pressures.

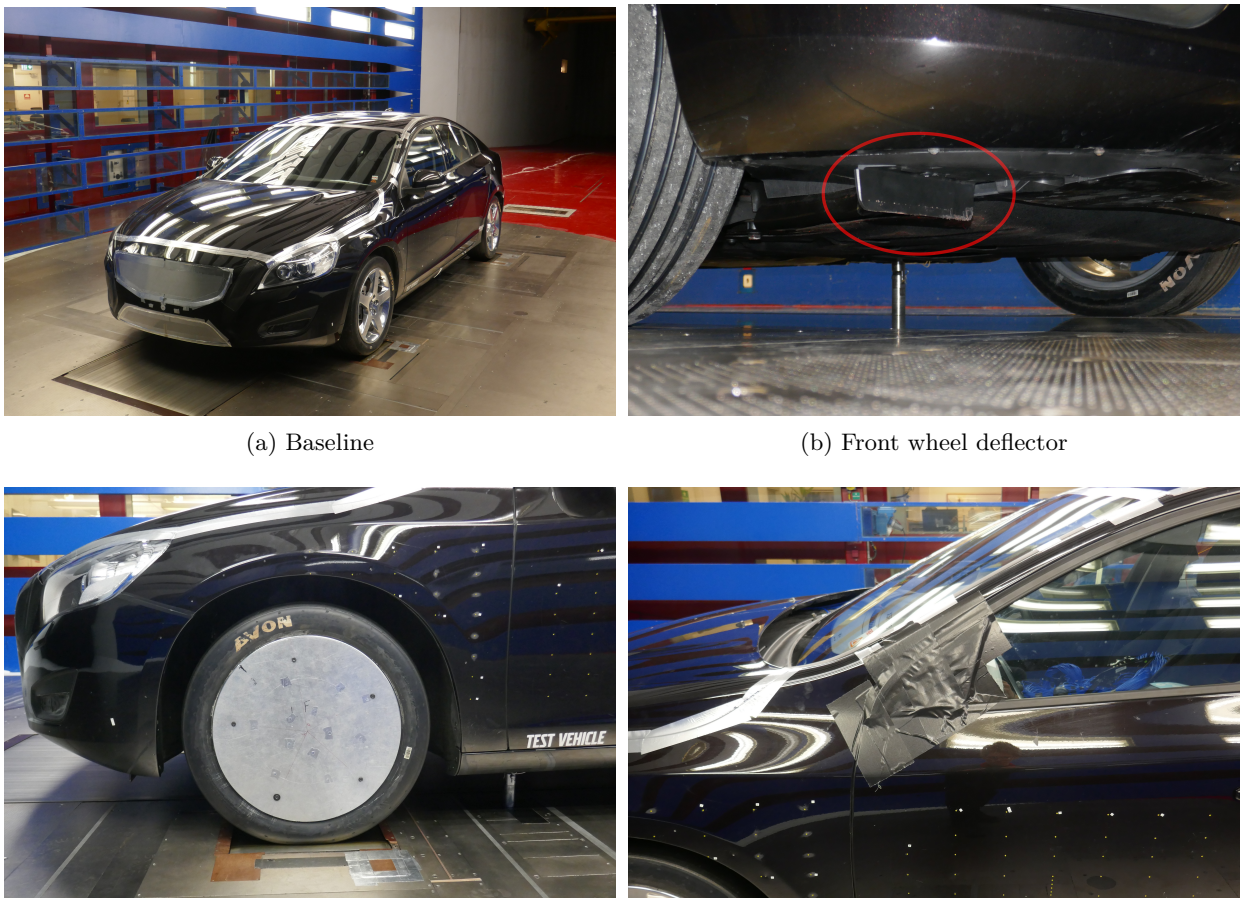

(a) Baseline

(b) Front wheel deflector

(c) Covered rims

(d) No mirrors

Figure 2: The test object and the tested configurations.

For the simulations of the vehicle inside the wind tunnel, a numerical model of the physical wind tunnel was used. The domain has previously been described in the literature [7, 8, 10, 18, 19], and can be seen in Figure 3b. It consists of the full high-speed leg of the wind tunnel, from the settling chamber and contraction, via the full slotted test section including the plenum, to the first diffuser. The inlet of the domain was set as a mass flow inlet, with the mass flow adjusted such that the wind speed was 140 km/h at a point 1.2 m over the turntable center in the empty test section. This is the location for which the wind speed in the physical wind tunnel is calibrated. The outlet was placed at the end of an extension after the first diffuser and was set as a pressure outlet.

It shall be noted that using the mass flow tuned to match the empty tunnel in the simulations with a vehicle inside the test section is expected to result in a velocity in the test section that differs from the desired. This can be corrected by either adjusting the mass flow for the specific vehicle such that the pressure drop over the wind tunnel nozzle matches the empty test section simulations, or by calculating the actual test section velocity based on the nozzle pressure drop. In this work, the latter method was used, and the nominal test speed was calculated as

$$U_\infty = \sqrt{\frac{2k_q \Delta P}{\rho}}, \tag{1}$$

where k_q is a calibration constant from the wind tunnel commissioning, ΔP the pressure loss over the nozzle as measured by two pressure taps located in the settling chamber and near the nozzle exit, and ρ the air density. Furthermore, the reference pressure in the test section differs significantly from the pressure on the domain outlet mainly due to pressure recovery in the diffuser, and it is also affected by losses over the car and the wind tunnel test section. In this work, the test section reference pressure was calculated as

$$P_s = P_{C2} + k_p \Delta P, \tag{2}$$

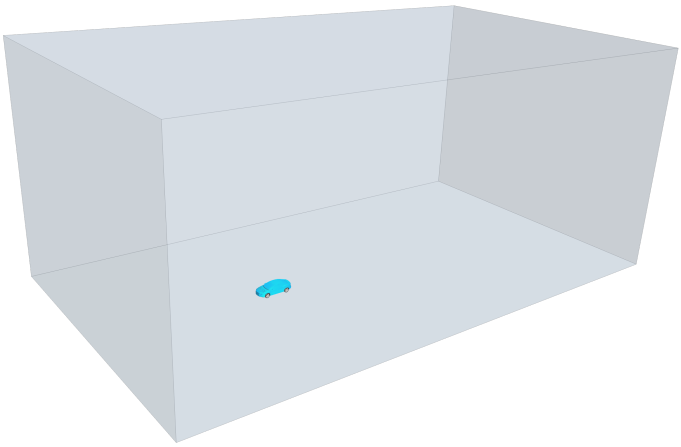

(a) Open road domain

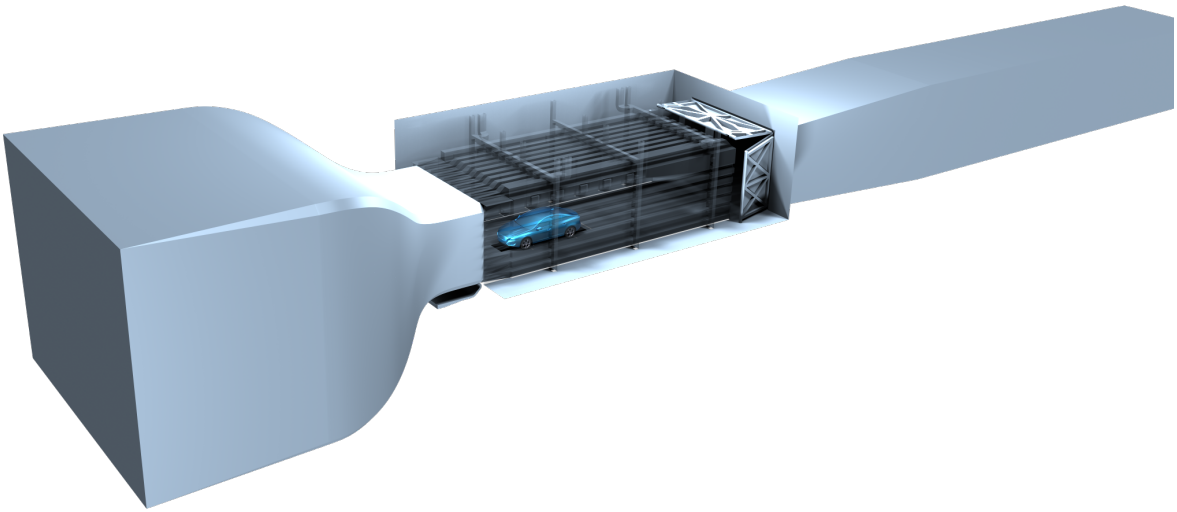

(b) Virtual model of the physical wind tunnel

Figure 3: The open road and virtual wind tunnel domains used. The two domains are not drawn to scale.

where P_{C2} is the pressure measured by the pressure tap at the nozzle exit, and k_p is another calibration constant from the commissioning. Both the wind speed and reference pressure determinations correspond to how these quantities are computed in the physical wind tunnel, with the difference that equation (1) was simplified to reflect the fact that the simulations are treating the air as incompressible. In order to ensure the correctness of the reference values, it was checked that the pressure coefficient at the stagnation point on the front of the vehicle matched $C_p = 1$, which is the case for the wind tunnel measurements. For non-dimensionalization of forces and pressures for the in-tunnel simulations, the nominal test speed and test section reference pressure were calculated according to equations (1) and (2), respectively.

All the ground effect simulation systems from the physical wind tunnel were taken into account in the simulations. A part of the suction scoop geometry was included in the simulation domain, and a mass flow inlet with the flow directed out of the domain was used as a boundary condition. The remaining systems were deemed too costly to resolve fully, and their respective influences were thus modeled using different boundary conditions set on the fully flat wind tunnel floor. For the distributed suction, the approach introduced by Cyr et al. [4] was used. In this approach, the patch to which the boundary condition is applied acts as a slip wall in the wall-tangential directions, but has a prescribed velocity through the wall in the normal direction, thus extracting air from the domain. All air removed from the domain by the scoop and the two distributed suction systems was reinjected back into the domain at the same locations as in the physical tunnel, meaning that the air from the scoop reentered the tunnel above the slotted roof, and the air from

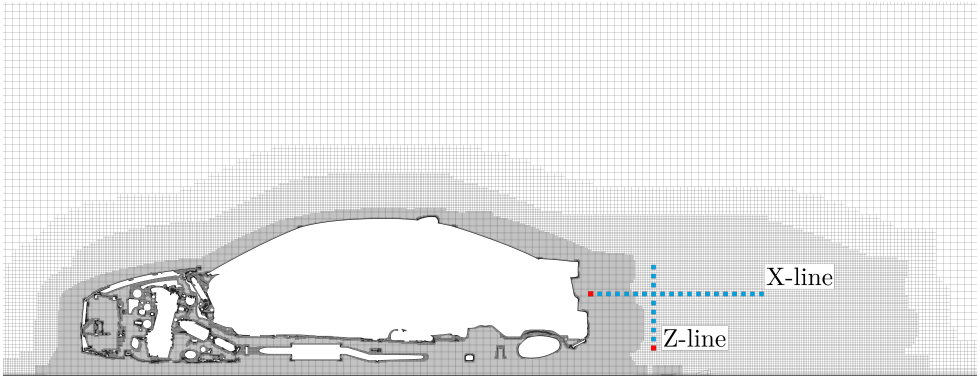

Figure 4: View of the mesh on the center plane around the vehicle, with the two sampling lines used for the two-point correlation.

the distributed suction was reinjected outside of the slotted walls. However, a fraction of the air extracted from the second distributed suction system was used to feed the tangential blowers, which is also in line with the setup of the physical tunnel.

The tangential blowers were modeled using an approach introduced by Olander [7], where a patch on the floor is set as a mass flow inlet with an inlet direction almost tangential to the floor. This method has previously been shown to give reasonable agreement with measurements of the boundary layer displacement thickness in the empty tunnel [20], both behind the blowers as well as outside their area of influence. The five belts were simulated using a moving wall boundary condition, and all small gaps around the belts, necessary to allow the belts to rotate, were ignored. Ideally, the full WDU installation consisting of belts, rollers, and motors would be simulated, together with the balance room in which everything but the top surface resides. However, this would increase the complexity of the simulations to an extent that is infeasible using the available resources.

2.2.2 Inclusion of the lift acting on the wheel drive units

As described in Section 2.1, a spurious lift component acts on the wheel drive units in the physical measurements. To achieve a one-to-one comparison between the uncorrected physical test data and the in-tunnel simulations, this additional lift has to be accounted for in the simulation results. Thus, for the simulations denoted "PVT CFD WDU" in Section 3.1, the pressure was integrated over each WDU patch and the resulting force added to the front- or rear lift force on the vehicle. This procedure assumes that the pressure acting on the lower side of the WDU equals the reference pressure in the test section. In the physical tunnel, a small difference has been measured between these pressures, which would amount to an error on the order of one lift count.

2.2.3 Meshing

The meshes were of trimmed cell type with prism layers on all no-slip boundaries. The surface cell sizes were in the range of 1 mm to 8 mm on the tophat and 2 mm to 4 mm on the underbody and in the engine bay. The boundary layer was resolved with up to 12 prism layers on the tophat, muffler and underbody panels, resulting in y^+-values below unity, while the rest of the underbody and underhood were meshed with a single prism layer, resulting in y^+ below 130. Volumetric refinements were added around the car in order to resolve the base wake and wheel wakes, with 8 mm cells used close to the car, and 16 mm cells further away. The mesh around the vehicle can be seen in Figure 4. In the open road simulations, the total mesh size was around 135 million cells.

For the wind tunnel geometry, up to 10 prism layers were used, resulting in $30 < y^+ < 150$ on the test section walls. The slot openings were resolved with 16 mm cells in order to achieve an accurate representation of the shear layer behavior. This has previously been shown to have a significant impact on the flow in the downstream half of the test section [10]. The inclusion of the wind tunnel geometry resulted in a significant increase in the number of cells to a total of around 340 million.

In order to evaluate the mesh resolution in the base wake, the two-point correlation of the longitudinal velocity was computed along the two sampling lines shown in Figure 4. The lines were chosen to represent

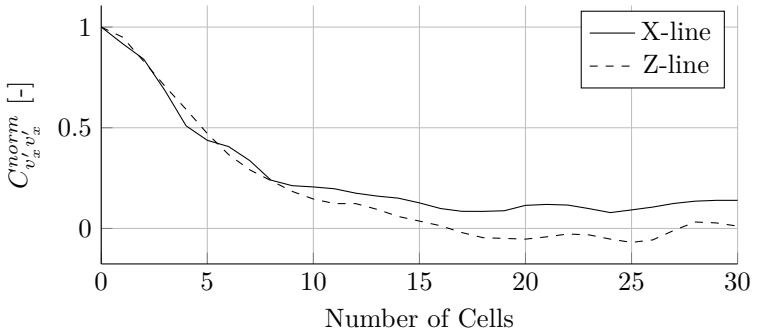

Figure 5: Normalized two-point correlation for the two sampling lines in the wake.

two directions as well as covering areas with different mesh resolution, which is similar to the setup used by Urquhart et al. [21] for a comparable vehicle geometry. The normalized two-point correlation of the fluctuating velocity in the longitudinal direction is defined as

$$C^{norm}_{v'_x v'_x}(x_A, x_B) = \frac{\overline{v'_x(x_A) v'_x(x_B)}}{v'_{x,RMS}(x_A) v'_{x,RMS}(x_B)},$$

where v'_x denotes the fluctuating part of the longitudinal velocity v_x, and $v'_{x,RMS}$ its root mean square. The spatial coordinates of interest are denoted x_A and x_B. Davidson [22] concluded that this is a better measure of LES resolution than considering the energy spectra or fraction of resolved to unresolved turbulent kinetic energy, and that the largest eddies should be resolved by at least eight cells for a coarse LES. This corresponds to having a correlation above zero at a separation distance of more than eight cells. As can be seen in Figure 5, which shows the normalized two-point correlation for the two sampling lines, the correlation spans over more than 10 cells for both lines. This indicates that the mesh resolution is adequate for a coarse LES, and thereby also sufficient for the IDDES method. In order to compute the two-point correlations, the first cell along each line was used as the reference cell (x_A), as shown in red in Figure 4.

3 Results and discussion

The findings from the performed measurements and simulations are presented and discussed in this section, beginning with a comparison of the absolute non-dimensional forces on the vehicle. This is followed by a look into the prediction of force coefficient differences between configurations, after which open road and in-tunnel simulation results are compared.

3.1 Prediction of force coefficients

A comparison of the force coefficients can be seen in Figure 6. For confidentiality reasons, each absolute force coefficient presented has been given an arbitrary offset. "Corrected PVT" and "Uncorrected PVT" denote physical measurements with and without blockage correction applied, while "Open road CFD" and "PVT CFD" denote simulations in open road conditions and using the wind tunnel geometry as the computational domain, respectively. "PVT CFD WDU" refers to values including the lift on the wheel drive units (WDU). For all forces and configurations, the open road CFD should be compared to the corrected measurement data, and the wind tunnel CFD to the uncorrected data. With perfect simulations and a perfect correction method, both these comparisons would show zero difference. In the case of matching values between the uncorrected measurements and simulations of the car inside the tunnel, but differences between corrected values and open road simulations, it is likely that the correction procedure used for the physical measurements is not able to fully correct for the wind tunnel interference effects.

Figure 6a shows that drag prediction is significantly improved by including the wind tunnel geometry in the simulations for all investigated cases. For both the baseline case and the case without front wheel deflectors, the tunnel simulations result in a drag coefficient matching the uncorrected measurements. With covered rims, and for rearview mirrors removed, the tunnel simulations give drag values that are 5 counts ($\Delta C_d = 0.005$) higher than the uncorrected tunnel values. This is just outside the repeatability of the physical measurements, which is within 3 counts, as given in Table 1. The improvement in drag prediction aligns well with the results of the base pressure measurements seen in Figure 7. It can be seen that the base pressure from the open road simulations is overall higher than what is measured in the wind tunnel. For the in-tunnel simulations, the overall pressure is better predicted, even though some differences still occur. Especially in the lower right region, the simulations show a lower pressure than the measurements. This can be partly explained by the pressure taps being slightly misplaced in this area.

Assuming that the good agreement between uncorrected measurements and tunnel simulations can be seen as a validation of the CFD method, it is very likely that the correction method used for the physical measurements underpredicts the boundary interference effects. This can be seen from the fact that the open road CFD shows drag values of about 9 to 14 drag counts lower than the corrected measurements, which are supposed to reflect open road conditions.

Considering the front and rear lift coefficients displayed in Figures 6b and 6c, it can be seen that the prediction of front lift is very poor for both simulation domains. For the rear, prediction quality is not improved by the inclusion of the wind tunnel domain. Part of this difference between simulations and measurements can be explained by the fact that the acceleration of the flow around the wheels near the contact with the ground results in suction on the wheel drive units, which is reflected in the physical measurements as an increase in lift.

By including this lift acting on the wheel drive units in the simulations of the car inside the tunnel, the prediction of front lift is improved, as can be seen for the bars denoted "PVT CFD WDU" in Figure 6. However, with the inclusion of the WDU lift, the rear lift coefficient becomes significantly overpredicted, despite the fact that the magnitude of the suction on the rear WDUs are roughly half compared to the front due to the front wheel being subjected to the freestream flow resulting in a stronger acceleration around the contact patch. When considering the total lift on the car shown in Figure 6d, it is found that the inclusion of the wind tunnel geometry and correction for the WDU lift generally results in an overprediction of the total lift compared to experiments, with the covered rims configuration as an exception. This underprediction likely stems from a misprediction of the flow field close to the contact patch, affecting the pressure on the WDU and on the wheel itself. Difficulties predicting the behavior of fully covered rims on vehicles of sedan type have previously been noted for open road simulations [14, 15, 23]. Hobeika and Sebben [15] hypothesized that the flow influence from the rotating rims dominates the flow behavior for the open rim case, while the roughness of the tire sidewall has a larger influence for the closed rim. Thus, treating the sidewall as a smooth surface in the simulations, as was done in the present work, would result in a larger error for the closed rim.

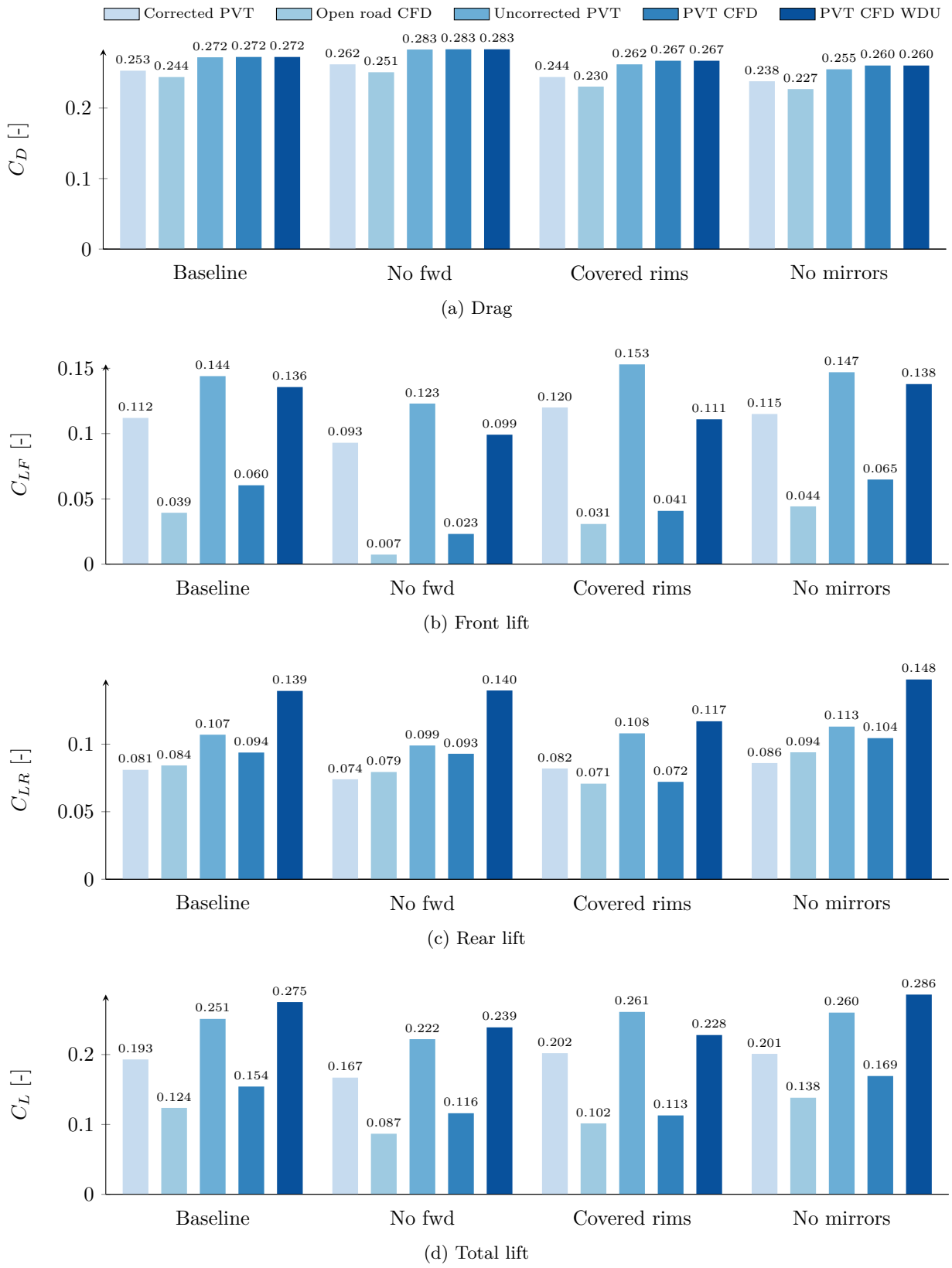

Figure 6: Comparison of drag and lift coefficients between the wind tunnel and simulations. All coefficients have been offset for confidentiality.

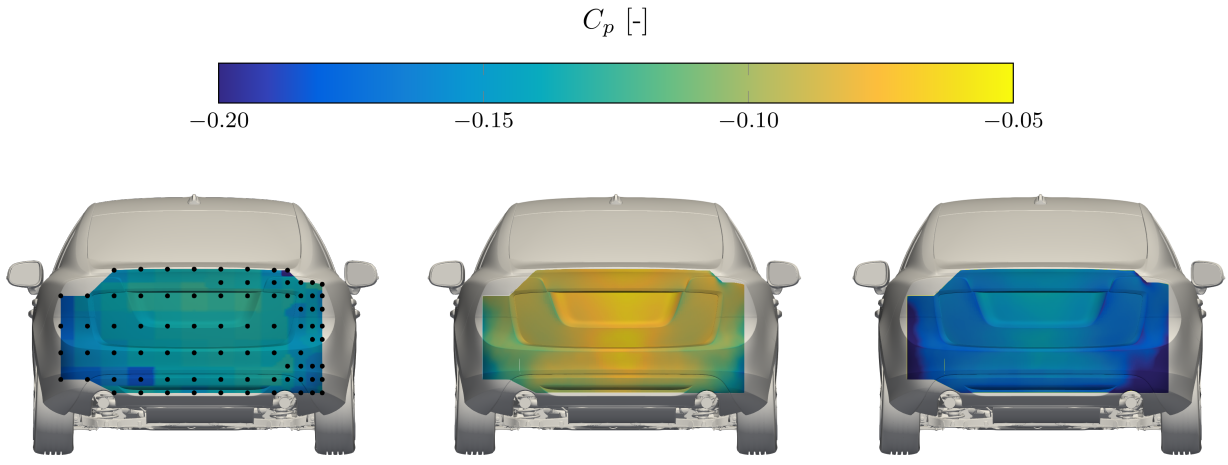

(a) Physical measurement. Black dots mark measurement positions.

(b) Open road CFD

(c) PVT CFD

Figure 7: Base pressure distribution on the vehicle in its baseline configuration from measurements (a), and simulations (b) and (c).

As noted in Section 2.1, the correction method for the physical measurements includes a correction for the WDU lift based on simplified CFD simulations of slick tires on a wheel drive unit [11]. When this method was derived, it was found that the CFD overpredicted the lift on the WDUs, which was also in line with the findings in a previous study by Wickern and Beese [24]. Hence, it is plausible that the present method also results in a too high lift from the suction on the wheel drive unit, which would explain the overprediction of the total lift in the corrected simulations, but most likely not the shifted lift balance. This phenomenon can be caused by a number of effects, from insufficiencies in the CFD prediction of the flow field around the contact patch between the tires and the WDUs, to the fact that the geometry of the WDUs has been simplified to patches on the completely flat floor in the simulations. In the physical tunnel, there are small gaps around the belts and rollers to allow for some movement and to assure that no parts connected to the underfloor balance come in contact with the floor which may result in an unwanted load transfer. These gaps would allow for some leakage between the test section and the balance room located under it, resulting in a tendency for the pressures to equalize, which would decrease the lift on the wheel drive unit. Eng [11] found that the measured influence of the WDU lift was about 80 % of that found using CFD simulations. If applied to the lift on the wheel drive units in the in-tunnel simulations in this work, it would amount to a reduction of $\Delta C_L \approx -0.020$, which would result in a good prediction of the total lift for all but one of the investigated configurations.

Further insights into the behavior of the lift coefficients can be provided by the centerline pressure profiles shown in Figure 8. It can be seen that the pressure is generally lower for the in-tunnel simulations compared to the open road case, indicating a higher overall lift force. This is consistent with the integrated forces in Figure 6. However, it is not clear from the centerline pressures why the lift balance from the simulations deviates so much from the test values. Over the windscreen and rear window, the inclusion of the tunnel geometry improves the pressure predictions, while the open road simulations seem to provide slightly better accuracy over the hood and boot lid. Except for what is believed to be outliers due to measurement errors stemming from damaged pressure holes at one location on the roof and two at the boot lid, the largest discrepancy between the measured and simulated pressures can be seen around the front of the roof, at $x \approx 2\,\mathrm{m}$. This can likely be attributed to the fact that the physical model had a tape strip smoothing over the joint between the windscreen and the roof, while the numerical model had a small step here, resulting in a local flow acceleration. Given the overall good agreement of the pressure on the centerline of the tophat, it is believed that the poor prediction of the lift balance stems from issues of the underbody flow prediction.

3.2 Prediction of force coefficient differences

The force coefficient differences between the respective configurations and the baseline can be seen in Figure 9. Comparisons are only shown within the same simulation or test method, that is, “Corrected PVT”

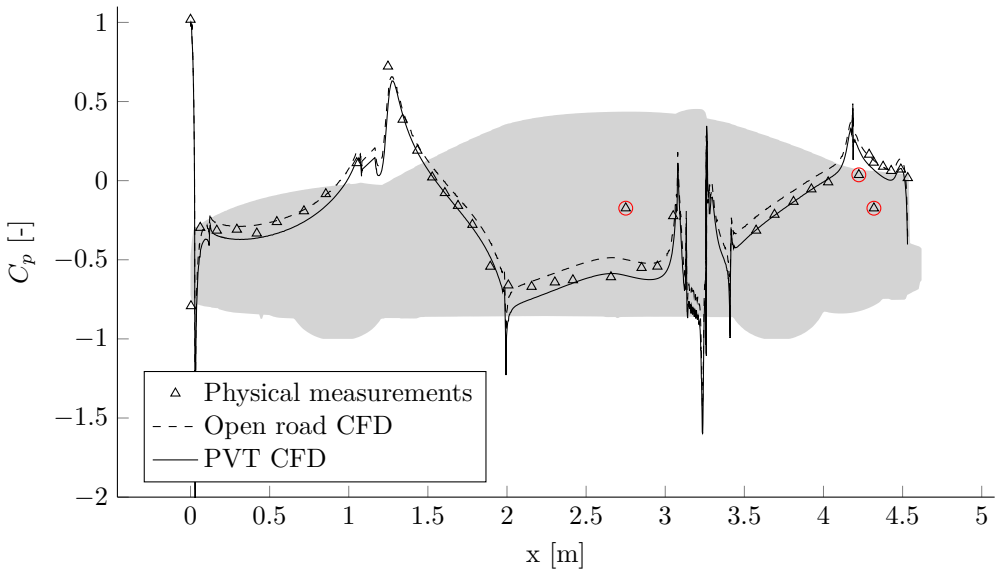

Figure 8: Centerline pressure profile on the tophat for the baseline configuration. The suspected damaged pressure taps marked with red circles.

is compared to baseline "Corrected PVT", "PVT CFD" to baseline "PVT CFD", and so on. It can be seen that the drag increase from removing the front wheel deflector is well predicted for both simulation methods. For the remaining two configurations, the drag delta is predicted to within $\Delta\Delta C_D = 0.005$ for all CFD methods. It is interesting to note that the drag delta is overpredicted by the open road CFD and underpredicted by the in-tunnel simulations for both the covered rims and the configuration without a mirror. As noted in Section 3.1, the behavior of the covered rims case is likely caused by inaccuracies in the flow field predictions in the simulation. Furthermore, since the mounting points for the mirrors were covered over with tape in the wind tunnel, the geometry used to represent this case in the simulations did not exactly match that of the physical tunnel, possibly causing differences in the predicted flow field. These mispredictions are most likely affected by the blockage effects introduced by the wind tunnel geometry, thus resulting in the drag delta being overpredicted by the open road simulations and underpredicted by the in-tunnel simulations.

For the prediction of the lift deltas, it can be seen that the small front- and rear lift changes for the case without rearview mirrors are well predicted, especially with the in-tunnel setup. However, the predictions of the deltas for the two cases that alter the underbody flow (no fwd, covered rims) are less satisfying. This further strengthens the belief that the misprediction of the lift balance stems from the prediction of the underbody flow. The results for the covered rims are particularly interesting since the delta from CFD is of the opposite sign compared to the physical measurements. This situation was not improved by including the wind tunnel and got even worse when correcting for the lift on the wheel drive units. However, leaving the WDU lift out of any comparison between in-tunnel simulations and uncorrected measurement data is not an option, since it will inevitably be part of the lift measured in the physical tunnel.

3.3 Comparison between open road and wind tunnel simulations

As was seen in Figure 7, the higher drag seen in the wind tunnel simulations compared to their open road counterpart is reflected in a drop in base pressure. This is further emphasized by Figure 10, which shows the surface pressure difference between in-tunnel and open road simulations for the baseline configuration. As expected due to the blockage effects, the overall pressure on the vehicle surface is lower for the in-tunnel setup, while the stagnation pressure in the front is not affected by the simulation domain. This is also in line with the centerline pressure profiles in Figure 8. The most visible differences seen in Figure 10 occur in areas of strong acceleration, for example the front edge of the hood, over the rearview mirrors and a-pillars, and around the front tires. The tires show an interesting behavior, where the pressure difference suddenly vanishes at the separation line along the side of the tire. A local increase can also be seen near the contact patch. The cause of this increase is likely that the vortex emanating from the contact patch is pushed closer to the body by blockage effects for the in-tunnel setup.

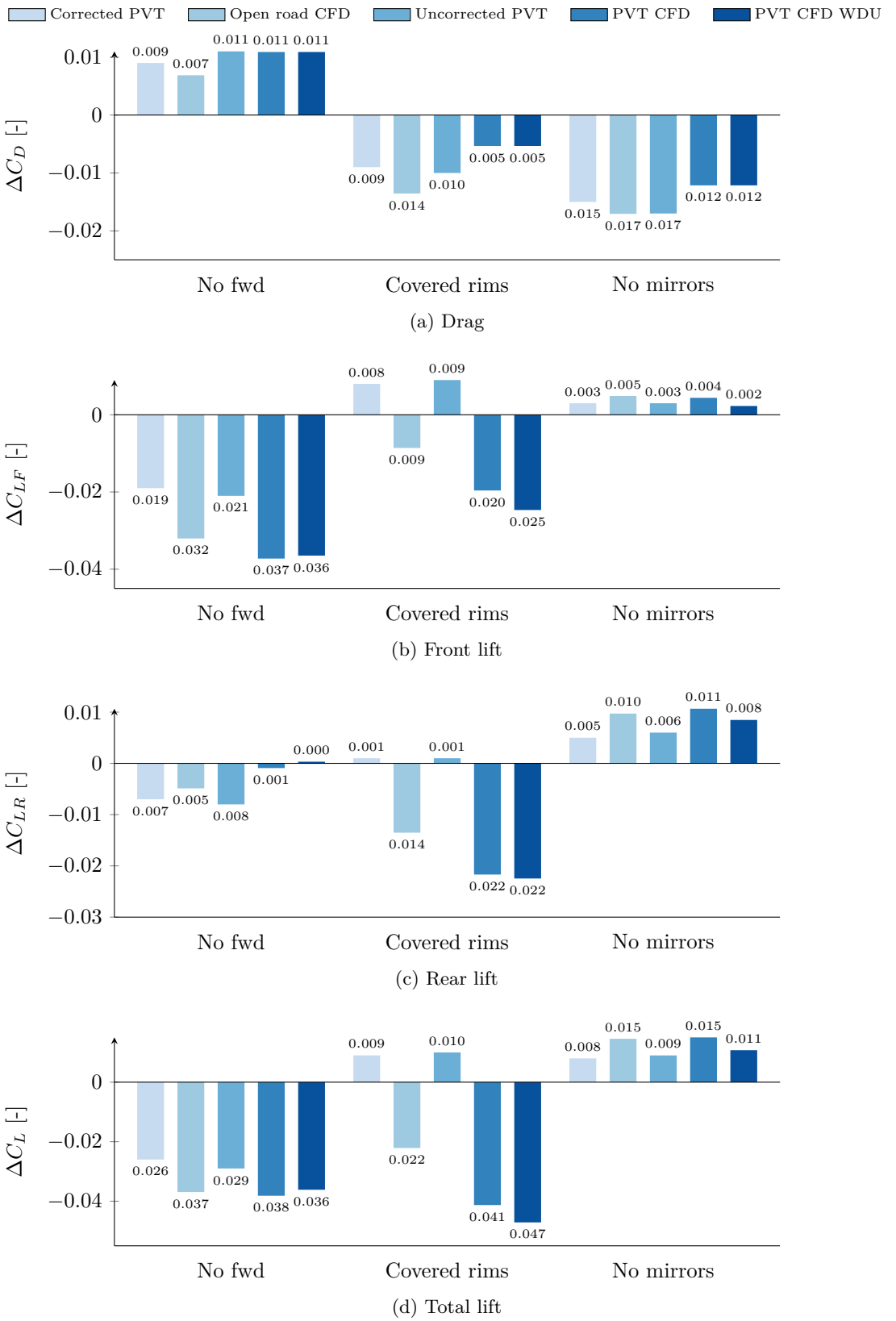

Figure 9: Differences in drag and lift compared to baseline for all configurations. The numeric labels show the magnitude of the change rounded to three decimal places.

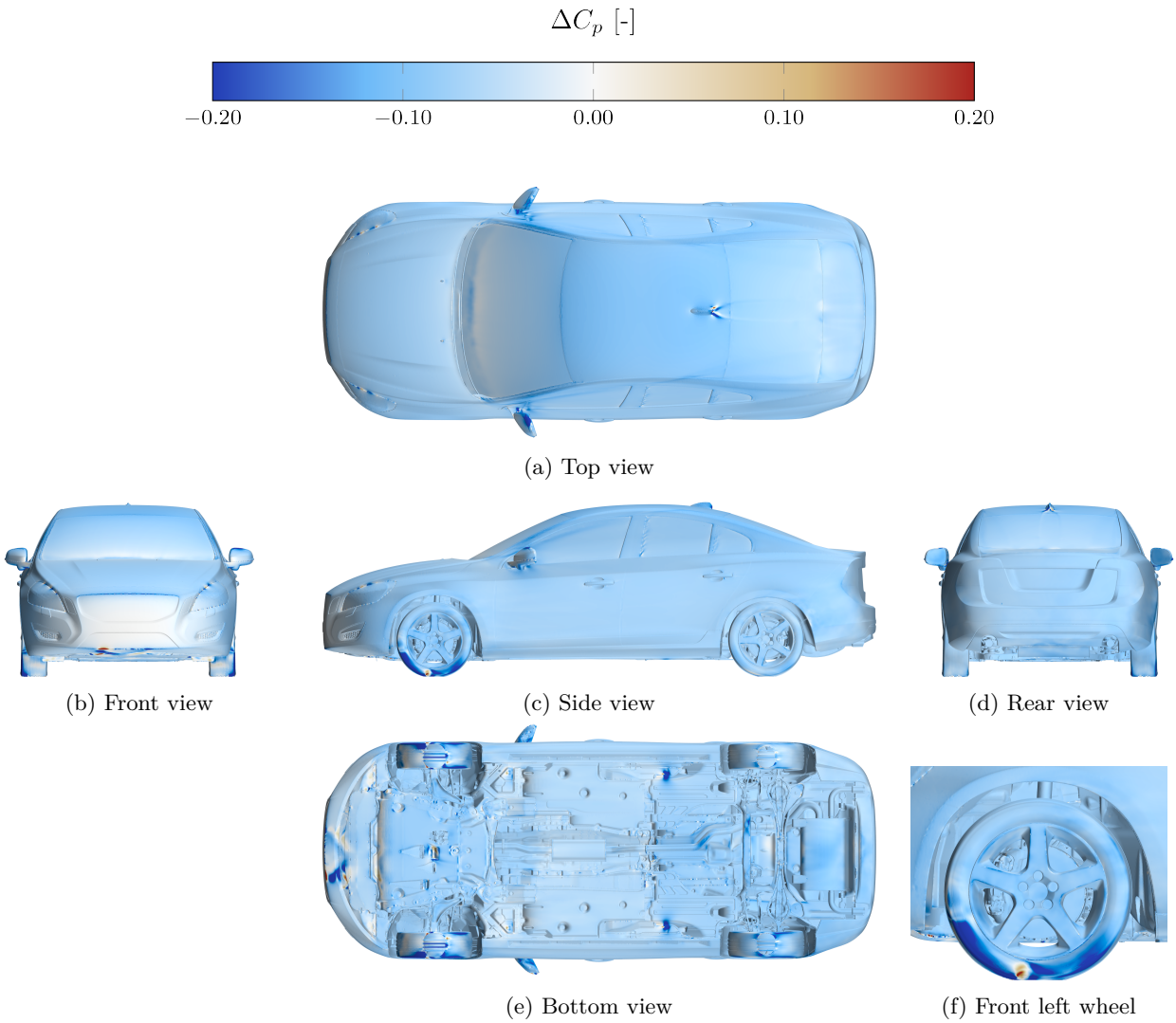

(a) Top view

(b) Front view

(c) Side view

(d) Rear view

(e) Bottom view

(f) Front left wheel

Figure 10: Pressure difference between in-tunnel and open road simulations for the baseline configuration. A positive difference indicate higher pressure for the in-tunnel simulation.

An area showing a pressure difference behavior not consistent with the overall trend of more or less uniformly lower pressure for the in-tunnel simulations is the underside of the front lip and leading edge of the engine undershield. Around the front lip, a patch of lower pressure can be seen for the in-tunnel simulations, which is caused by a different separation prediction. This is probably caused by the difference between the fully moving ground plane used in the open road simulation, and the modeled physical five belt system in the wind tunnel. This area of the vehicle is affected by the pressure gradient introduced by the distributed suction, which may cause different separation behavior.

These local differences raise questions to whether the global correction methods that are currently employed can be adjusted to not only give reasonable open road-equivalent data for most configurations but to also take local effects into account. This is something that needs to be investigated in more depth, and where simulation methods like those employed in this paper will be instrumental in order to understand how to improve the corrections.

4 Conclusions

The effect of including the wind tunnel geometry and its associated boundary conditions in numeric simulations of the aerodynamic forces on a vehicle of sedan type has been investigated. Based on the results obtained, it is concluded that a very good prediction of the absolute drag coefficient is possible by including the wind tunnel geometry in CFD simulations and comparing to uncorrected data from the wind tunnel. A key component to achieve this was to compute the non-dimensionalized quantities in the in-tunnel simulations in the same way as it is done in the physical tunnel, meaning that the reference pressure and the nominal velocity in the test section were calculated based on the pressure drop over the wind tunnel nozzle.

Despite the good agreement in drag, prediction of lift is still not completely satisfactory. Reasonable agreement between uncorrected measurements and in-tunnel simulations was found for the total lift force when taking the lift force acting on the wheel drive units into account. Yet, the balance between front and rear lift did not match that found in the wind tunnel. It is believed that part of the misprediction stems from an overprediction of the wheel drive unit lift; a phenomenon that has been previously reported in the literature.

When considering changes in drag between different configurations of the vehicle, the inclusion of the wind tunnel geometry did not yield a significant improvement of the prediction quality compared to the open road simulations. However, for some configurations, the open road simulations tend to exaggerate the differences, while the in-tunnel simulations show a smaller delta than the wind tunnel measurements.

For the prediction of lift deltas, it was found that the agreement between simulations and wind tunnel was good for the configuration consisting of changes to the tophat of the vehicle, while the configurations altering the underbody flow resulted in worse prediction quality. This is in line with results showing good agreement of the centerline pressure on the tophat when the vehicle is simulated inside the wind tunnel, and further indicates that the misprediction of lift most likely stems from the simulation quality of the underbody flow.

By comparing the difference in surface pressure between open road and in-tunnel simulations, it was found that the normalization procedure used for the wind tunnel simulations was correct in that it resulted in the same pressure coefficient at the stagnation region at the front of the vehicle for both simulation domains. Furthermore, it showed that the blockage effects in the wind tunnel result in an overall lower pressure on the surface of the vehicle, which explains the higher drag seen in the uncorrected wind tunnel measurements. However, in areas of strong acceleration, larger differences were seen, and some separations were differently predicted in the two different domains. This raises questions on the applicability of global correction methods when investigating local changes, and warrants more investigation.

References

[1] O. Fischer, T. Kuthada, N. Widdecke, and J. Wiedemann. "CFD Investigations of Wind Tunnel Interference Effects". In: *SAE Technical Paper 2007-01-1045*. Apr. 16, 2007. DOI: 10.4271/2007-01-1045.

[2] O. Fischer, T. Kuthada, J. Wiedemann, P. Dethioux, R. Mann, and B. Duncan. "CFD Validation Study for a Sedan Scale Model in an Open Jet Wind Tunnel". In: *SAE Technical Paper 2008-01-0325*. Apr. 14, 2008. DOI: 10.4271/2008-01-0325.

[3] O. Fischer, T. Kuthada, E. Mercker, J. Wiedemann, and B. Duncan. "CFD Approach to Evaluate Wind-Tunnel and Model Setup Effects on Aerodynamic Drag and Lift for Detailed Vehicles". In: *SAE Technical Paper 2010-01-0760*. Apr. 12, 2010. DOI: 10.4271/2010-01-0760.

[4] S. Cyr, K.-D. Ih, and S.-H. Park. "Accurate Reproduction of Wind-Tunnel Results with CFD". In: *SAE Technical Paper 2011-01-0158*. Apr. 12, 2011. DOI: 10.4271/2011-01-0158.

[5] C. Collin, S. Mack, T. Indinger, and J. Mueller. "A Numerical and Experimental Evaluation of Open Jet Wind Tunnel Interferences using the DrivAer Reference Model". In: *SAE International Journal of Passenger Cars - Mechanical Systems* 9.2 (Apr. 5, 2016). ISSN: 1946-4002. DOI: 10.4271/2016-01-1597.

[6] S. Perzon. "On Blockage Effects in Wind Tunnels – A CFD Study". In: *SAE Technical Paper 2001-01-0705*. Mar. 5, 2001. DOI: 10.4271/2001-01-0705.

[7] M. Olander. "CFD Simulation of the Volvo Cars Slotted Walls Wind Tunnel". Masters Thesis. Chalmers University of Technology, 2011.

[8] A. Wall. "Simulating the Volvo Cars Aerodynamic Wind Tunnel with CFD". Masters Thesis. Chalmers University of Technology, 2013.

[9] J. Sternéus, T. Walker, and T. Bender. "Upgrade of the Volvo Cars Aerodynamic Wind Tunnel". In: *SAE Technical Paper 2007-01-1043*. Apr. 16, 2007. DOI: 10.4271/2007-01-1043.

[10] E. Ljungskog. "Investigations of Flow Conditions in an Automotive Wind Tunnel". Licentiate Thesis. 2017.

[11] M. Eng. "Investigation of Aerodynamic Correction Methods Applied to a Slotted Wall Wind Tunnel". Masters Thesis. Technische Universität Berlin, Mar. 23, 2009.

[12] T. Hobeika. "Wheel Modelling and Cooling Flow Effects on Car Aerodynamics". Doctoral thesis. Chalmers University of Technology, 2018.

[13] S. Bonitz. "Development of Separation Phenomena on a Passenger Car". Doctoral thesis. Chalmers University of Technology, 2018.

[14] T. Hobeika and S. Sebben. "CFD investigation on wheel rotation modelling". In: *Journal of Wind Engineering and Industrial Aerodynamics* 174 (Mar. 1, 2018), pp. 241–251. ISSN: 0167-6105. DOI: 10.1016/j.jweia.2018.01.005.

[15] T. Hobeika and S. Sebben. "Tyre Pattern Features and Their Effects on Passenger Vehicle Drag". In: *SAE International Journal of Passenger Cars - Mechanical Systems* 11.5 (Apr. 3, 2018), pp. 401–413. ISSN: 1946-4002. DOI: 10.4271/2018-01-0710.

[16] M. L. Shur, P. R. Spalart, M. K. Strelets, and A. K. Travin. "A hybrid RANS-LES approach with delayed-DES and wall-modelled LES capabilities". In: *International Journal of Heat and Fluid Flow* 29.6 (Dec. 2008), pp. 1638–1649. ISSN: 0142-727X. DOI: 10.1016/j.ijheatfluidflow.2008.07.001.

[17] P. Ekman, T. Larsson, T. Virdung, and M. Karlsson. "Accuracy and Speed for Scale-Resolving Simulations of the DrivAer Reference Model". In: WCX SAE World Congress Experience. Apr. 2, 2019, pp. 2019–01–0639. DOI: 10.4271/2019-01-0639.

[18] E. Ljungskog, S. Sebben, A. Broniewicz, and C. Landström. "A parametric study on the influence of boundary conditions on the longitudinal pressure gradient in CFD simulations of an automotive wind tunnel". In: *Journal of Mechanical Science and Technology* 31.6 (June 1, 2017), pp. 2821–2827. ISSN: 1738-494X, 1976-3824. DOI: 10.1007/s12206-017-0525-2.

[19] E. Ljungskog, S. Sebben, and A. Broniewicz. "Uncertainty Quantification of Flow Uniformity Measurements in a Slotted Wall Wind Tunnel". In: *SAE Technical Paper 2019-01-0656*. Apr. 2, 2019. DOI: 10.4271/2019-01-0656.

[20] E. Ljungskog, S. Sebben, A. Broniewicz, and C. Landström. "On the Effects of Wind Tunnel Floor Tangential Blowing on the Aerodynamic Forces of Passenger Vehicles". In: *SAE International Journal of Passenger Cars - Mechanical Systems* 10(2).2017 (2017). DOI: 10.4271/2017-01-1518.

[21] M. Urquhart, S. Sebben, and L. Sterken. "Numerical analysis of a vehicle wake with tapered rear extensions under yaw conditions". In: *Journal of Wind Engineering and Industrial Aerodynamics* 179 (Aug. 1, 2018), pp. 308–318. ISSN: 0167-6105. DOI: 10.1016/j.jweia.2018.06.001.

[22] L. Davidson. "Large Eddy Simulations: How to evaluate resolution". In: *International Journal of Heat and Fluid Flow*. The 3rd International Conference on Heat Transfer and Fluid Flow in Microscale 30.5 (Oct. 1, 2009), pp. 1016–1025. ISSN: 0142-727X. DOI: 10.1016/j.ijheatfluidflow.2009.06.006.

[23] S. Koitrand, A. Gaylard, and G. O. Fiet. "An Investigation of Wheel Aerodynamic Effects for a Saloon Car". In: *Progress in Vehicle Aerodynamics and Thermal Management: Proceedings of the 10th FKFS-Conference*. Renningen: Expert-Verlag, 2015. ISBN: 978-3-8169-3322-9.

[24] G. Wickern and E. Beese. "Computational and Experimental Evaluation of a Pad Correction for a Wind Tunnel Balance Equipped for Rotating Wheels". In: SAE 2002 World Congress & Exhibition. Mar. 4, 2002. DOI: 10.4271/2002-01-0532.

Acknowledgements

This work was funded by FFI (*Fordonsstrategisk Forskning och Innovation*, Strategic Vehicle Research and Innovation) through Vinnova (Sweden's innovation agency), and Volvo Cars.

The simulations were performed on resources provided by the Swedish National Infrastructure for Computing (SNIC) at The National Supercomputer Centre in Sweden (NSC) and Chalmers Centre for Computational Science and Engineering (C3SE).